Dalton Transactions

PAPER

Cite this: *Dalton Trans.*, 2018, **47**, 13849

Developing a magnetic metal organic framework of copper bearing a mixed azido/butane-1,4-dicarboxylate bridge: magnetic and gas adsorption properties†

Azam Hassanpoor,[a] Masoud Mirzaei, *[a] Mahdi Niknam Shahrak [b] and Anna M. Majcher [c]

A magnetic metal organic framework $\{[Cu(but\text{-}1,4\text{-}dc)_{0.5}(N_3)(H_2O)]\cdot H_2O\}_n$ (**MFUM-1(Cu)**) (but-1,4-dc = butane-1,4-dicarboxylate) was synthesized and characterized structurally and magnetically. In MFUM-1(Cu), each Cu^{II} ion has a distorted octahedral geometry with an obvious Jahn–Teller distortion, where the coordination environment is composed of mixed EO-azido/aliphatic based carboxylate/H_2O threefold bridges. These bridges extend the structure of MFUM-1(Cu) in two dimensions by covalent connectivity and form square-shaped channels. Also, a study was done to determine the effectiveness of sonochemical synthesis for the preparation of nano-sheets of MFUM-1(Cu) and subsequently the influence of particle size on physical properties such as magnetic behavior and thermal stability. The particles were characterized by elemental analyses, infrared spectroscopy (IR), scanning electron microscopy (SEM), thermogravimetric analysis (TGA), and powder X-ray diffraction (PXRD) analyses. The effects of parameters such as concentration, solvent, and reaction time on the size distribution, morphology, and yield of product were carefully studied. The magnetic properties of MFUM-1(Cu) and corresponding nano-structure were examined which indicated metamagnetism with strong intrachain ferromagnetic coupling *versus* the weak interchain antiferromagnetic coupling. Finally, the application of MFUM-1(Cu) in the separation of carbon dioxide from nitrogen and also from methane was theoretically investigated. High calculated selectivity of CO_2 over N_2 and CH_4 reveals the potential application of MFUM-1(Cu) in practical systems of gas separation.

Received 21st July 2018,
Accepted 12th September 2018

DOI: 10.1039/c8dt02986e

rsc.li/dalton

1. Introduction

In past decades, great efforts have been devoted to the rational design and synthesis of magnetic coordination polymers (CPs) and metal organic frameworks (MOFs) because they provide genuine opportunities to explore the fundamental aspects of magnetic interactions and magneto-structural correlations in molecular systems.[1] The general chemical strategy for the construction of molecular magnets is based on the use of short bridging ligands that can effectively mediate the magnetic coupling between the local spin carriers (metal ions having unpaired electrons).[2] The most extensively used spin carriers are 3d transition metal ions such as Mn, Fe, Co, Ni and Cu.[3] For the bridges, the shorter and the more conjugated ligands are, the more efficient for transmitting coupling. Consequently, short bridges of one to three atoms, such as hydroxyl,[4] cyano,[5] azido,[6] oxalato/oxamate,[7] and carboxylate[8] are excellent ligands for obtaining discrete, one-, two-, or three-dimensional systems and take the key role in magnetic exchange between magnetic centres. Amongst them, the azido ligand has received considerable attention in this field because: (i) it is a most efficient ligand as regards the superexchange pathways between paramagnetic centres, (ii) it has great coordinative versatility which leads to a variety of structural types with the possibility of giving multi-dimensional compounds, and (iii) it can exhibit great coordinative versatility modes, such as μ-1,1 (end-on, *EO*), μ-1,3 (end-to-end, *EE*), μ-1,1,3, and others (see Scheme S1†) in which the magnetic exchanges are closely related.[9] Magneto-structural correlations for symmetric azido-bridged complexes have shown that two

[a]*Department of Chemistry, Faculty of Science, Ferdowsi University of Mashhad, Mashhad, Iran. E-mail: mirzaeesh@um.ac.ir*
[b]*Department of Chemical Engineering, Quchan University of Technology, Quchan 9477167335, I.R. Iran*
[c]*Department of Advanced Materials Engineering, Faculty of Physics, Astronomy and Applied Computer Science, Jagiellonian University, Łojasiewicza 11, 30-348 Kraków, Poland*

†Electronic supplementary information (ESI) available. CCDC 1551503 for **1**. For ESI and crystallographic data in CIF or other electronic format see DOI: 10.1039/c8dt02986e

main coordination modes *EO* and *EE*, can serve as good mediators for transmitting ferromagnetic (*FO*) interactions (mainly *EO*) or antiferromagnetic (*AF*) interactions (mainly *EE*).[1c] Of course, the type and the magnitude of the magnetic exchange interaction also depends on the detailed coordination geometries, such as the M–N_{azido}–M angle, the metal bridging ligand bond lengths M–N_{azido}, and the metal–metal separation.[10] The azido ligand can be further used to cooperate with the additional ligands to construct high dimensional magnetic coordination compounds with special structures and interesting properties. A search of the Cambridge Structural Database (CSD version 5.38/Feb 2017), produce a large number of coordination networks containing the azido bridge (1100 and 323 examples for *EO* and *EE* coordination modes respectively) where most of them have Cu, Ni, Mn, and Co as metal centres. The additional ligands in most of the reported structures are neutral nitrogen donor and mono alcoholic or carboxylate ligands but there are few examples of azido-bridged complexes containing dicarboxylate ligands. Combinations of dicarboxylate ligands with metal-azide systems is important from several perspectives. First, the carboxylate group in these ligands can act as a three-atom bridge and modify the magnetic properties.[11–13] Second, dicarboxylate ligands with various flexible coordination sites could form higher dimensional molecular nets.[14] Furthermore, nano-sized particles of CPs and MOFs are fascinating to explore, since they often exhibit new interesting size-dependent physical and chemical properties such as magnetism, luminescence, and thermal stability that cannot be observed in their bulk analogs.[15] Sonochemical processing has proven to be a useful technique for generating nano-particles of CPs and MOFs. Sonochemistry arises from the acoustic cavitation phenomenon, that is, the formation, growth, and implosive collapse of bubbles in a liquid. The extremely high temperatures (>5000 K), pressures (>20 MPa), and very high cooling rates (>107 K s^{-1}) attained during cavity collapse lead to many unique properties in the irradiated solution. These extreme conditions can drive chemical reactions, but they can also promote the formation of nano-sized particles, mostly by the instantaneous formation of a plethora of crystallization nuclei.[16,17] Additionally, these high dimensional porous coordination compounds exhibit important applications such as storage systems to trap and separate gas molecules.[18] Incorporation of functional sites within porous materials is a powerful strategy to improve the capacity and selectivity of CO_2 adsorption. Therefore, it is very beneficial to use some inorganic linkers with high ionic potential such as OH^-, CN^- and N_3^-, which create partial charges in structure and can induce strong interactions with gas molecules. Generally, the interactions between porous materials and gas molecules are typically van der Waals and electrostatic interactions.[18c] The adsorption capacity and selectivity of any adsorbent are the most significant properties relevant to adsorptive gas separation[18–20] and the adsorption isotherms of CO_2, N_2 and CH_4 gases are predicted using the Grand Canonical Monte Carlo (GCMC) method at 298 K and at various pressures up to 0.15 MPa. For post-combustion carbon capture from flue gas, nitrogen is the predominant gas among many other components[18,21] that CO_2 molecules should be separated from at 298 K and low pressure of the flue gas (*ca.* 1 atm). On the other hand, natural gas (CH_4) treatment is an essential process for natural gas upgrading in which some impurities such as CO_2 are efficiently separated from CH_4. As part of a continuing effort towards the preparation of CPs with various physical properties using different dicarboxylic acids,[22] in this work, we employed butane-1,4-dicarboxylate in the presence of a Cu/azide system. Our aim was to prepare multifunctional magnetic MOF and to investigate the effect of different co-ligands on the formation, structure and magnetic properties of the target complex. We successfully synthesized and structurally characterized one 2D-MOF formulated as $\{[Cu(but\text{-}1,4\text{-}dc)_{0.5}(N_3)(H_2O)]\cdot H_2O\}_n$ (MFUM-1(Cu)‡). To investigate the effect of particle size on the magnetic behavior and thermal stability, the nano-structure of MFUM-1(Cu) was prepared by sonochemical methods. Also, to achieve optimal conditions for the preparation of nano-structures of MFUM-1(Cu), we studied the effect of experimental parameters such as solvent, concentration and reaction time on the particle size, morphology, and yield of the sono-chemical product. The application of MFUM-1(Cu) as an adsorbent for CO_2 separation was also explored using GCMC simulation with a gas mixture including CO_2, N_2 and CH_4 selected for investigation of their adsorption capacities in compound **1**.

2. Experimental

2.1. Chemicals and apparatus

All reagents and solvents for the synthesis were commercially available and were used as received. The IR spectra in the 4000–400 cm^{-1} region were measured in KBr pellets on a PerkinElmer 580 spectrophotometer. Elemental analyses were carried out on a Thermo Finnigan Flash-1112EA microanalyzer. The TGA runs were taken on a TGA-50/50H standard type thermal analysis system. A multiwave ultrasonic generator (MisonixSonicator 4000 (S-4000), Qsonica, LLC, Newtown, CT, USA) equipped with a generator, converter, converter cable, a 1/2-inch replaceable tip horn, operating frequency at 20 kHz with a maximum power output of 600 (W) was used for the ultrasound irradiation. The wave amplitude in this experiment was 40 and ultrasonic energy dissipated was set at 5.96 W through the calorimetric method.[23] The size and morphology of nano-sheets of CP have been studied by SEM, a Leo 1450 VP, Germany. X-ray powder diffraction (XRD) measurements were recorded on a Philips diffractometer manufactured by X'pert with graphite monochromatized Cu-K_α radiation. Simulated XRD powder patterns were calculated by using Mercury based on the single crystal data. A suitable crystal of MFUM-1(Cu) was selected and (mounted on a nylon loop) on a

‡ Materials from Ferdowsi University of Mashhad-1 (Copper).

SuperNova, Dual, Cu at zero, Atlas diffractometer. The crystal was kept at 100.0(1) K during data collection. Using Olex2,[24] the structure was solved with the ShelXS[25] structure solution program using direct methods and refined with the ShelXL[25] refinement package using least squares minimisation. Data collection and refinement statistics are summarized in Table 1. Magnetic properties were measured using a Quantum Design MPMS 5XL SQUID magnetometer in magnetic field up to 50 kOe and at temperatures in the range between 1.8 and 300 K. Samples, in the form of powder, were pressed inside gelatin capsules and fitted into measurement straws without using additional adhesives. All DC measurements were corrected for the diamagnetic contribution of the sample holders and constituent atoms (Pascal's tables).[26]

2.1.1. Synthesis of{[Cu(but-1,4-dc)$_{0.5}$(N$_3$)(H$_2$O)]·H$_2$O}$_n$ (MFUM-1(Cu)). The high-quality crystals of MFUM-1(Cu) were prepared by the solvent diffusion method (Layering Technique). At first, an aqueous solution (5 mL) of $Cu(NO_3)_2{\cdot}3H_2O$ (61 mg, 0.25 mmol) was placed in a test tube. Then, 1 mL of mixture of water and ethanol solvents (1 : 1 v/v) was slowly dribbled into the tube so that two discrete layers formed. At the end, a mixture of H_2but-1,4-dc (40 mg, 0.25 mmol) and NaN_3 (16 mg, 0.25 mmol) in 8 mL ethanol was slowly dropped on the upper layer to form the third layer. Green rod single crystals of MFUM-1(Cu) were formed in the second layer after three days. Yield: 50% (based on Cu). Anal. calcd for $C_3H_8CuN_3O_4$: C, 16.86; H, 3.77; N, 19.67. Found: C, 17.53; H, 3.93; N, 20.48%. IR (KBr pellet, cm^{-1}): 3523–3400(b); 2091(s); 1548(s); 1404(m); 1302(m); 1135(w); 668(w).

2.1.2. Synthesis of MFUM-1(Cu) nano-structures by sonochemical process. To prepare the nano-structures of MFUM-1 (Cu), a 15 mL aqueous solution of $Cu(NO_3)_2{\cdot}3H_2O$ (0.05 M) was positioned in a high-density ultrasonic probe, operating at 20 kHz with a maximum power output of 600 W. Then, 16 mL of a solution containing organic acid (0.025 M) and NaN_3 (0.05 M) was added dropwise and the mixture was sonicated for 40 min. After synthesis, the sample was centrifuged and washed with water to remove excess reactant. Product (**A**): Yield: 70% (based on Cu). Anal. calcd for $C_3H_8CuN_3O_4$: C, 16.86; H, 3.77; N, 19.67. Found: C, 18.03; H, 3.82; N, 21.09%. IR (KBr pellet, cm^{-1}): 3407–3167(b); 2088(s); 1547(s); 1401(m); 1294(m); 1129(w); 678(w).

Detailed parametric studies are illustrated by seven representative experimental conditions (labeled A–G and summarized in Table 2). To study the effects of solvent, different solvents such as H_2O, H_2O/EtOH, and H_2O/CH_3CN were used in reactions A, B, and C. For reaction conditions A, D, and E, the concentration of reactants was changed. In addition, reaction times of 20, 40 and 60 min were tested for reactions F, A, and G.

Table 1 Selected crystallographic data and structure refinement parameters of MFUM-1(Cu)

Formula	$C_3CuH_8N_3O_4$
$D_{calc.}$/g cm^{-3}	2.016
μ/mm^{-1}	4.251
Formula weight	213.66
Color	Green
Shape	Rod
Size/mm^3	0.13 × 0.10 × 0.07
T/K	100.0(1)
Crystal system	Monoclinic
Space group	$C2/m$
a/Å	14.5619(4)
b/Å	6.4760(2)
c/Å	7.4973(2)
α/°	90
β/°	95.469(3)
γ/°	90
V/Å^3	703.80(3)
Z	4
Z'	0.5
Wavelength/Å	1.54184
Radiation type	Cu K$_\alpha$
Θ_{min}/°	6.106
Θ_{max}/°	76.260
Measured refl.	3958
Independent refl.	794
Reflections with $I > 2(I)$	773
R_{int}	0.0185
Parameters	64
Restraints	2
Largest peak	0.332
Deepest hole	−0.567
GooF	1.097
wR_2 (all data)	0.0657
wR_2	0.0654
R_1 (all data)	0.0246
R_1	0.0242

2.2. Computational procedure for adsorption equilibrium isotherms

Monte Carlo simulations in Grand Canonical (μ, V, T) ensemble were utilized to predict the adsorption equilibrium isotherms (adsorption capacity) of all components in the MFUM-1(Cu) framework at constant chemical potential, volume and temperature.[27] Also in this study GCMC simulations were performed with the assumption of rigid frameworks with atoms frozen at their crystallographic positions.[19] The universal force field (UFF) was employed to calculate the Lennard-Jones (LJ) potential parameters of adsorbates and adsorbent[28] coupled with 1×10^6 cycles to reach equilibrium. Moreover, in this study the charges of each atom in the adsorbent structure (atomic partial charges) were calculated *via* the Q equation[29] and the Peng–Robinson equation of state was

Table 2 Summary of synthesis conditions for the 7 samples of MFUM-1 (Cu) by sonochemical process

Samples/ conditions	Concentration (M) (Cu/L/NaN_3)	Solvent	Reaction time (min)
A	0.01, 0.005, 01	H_2O	40
B	0.01, 0.005, 01	H_2O/EtOH	40
C	0.01, 0.005, 01	H_2O/CH_3CN	40
D	0.05, 0.025, 0.05	H_2O	40
E	0.1, 0.05, 0.1	H_2O	40
F	0.01, 0.005, 01	H_2O	20
G	0.01, 0.005, 01	H_2O	60

"L" stands for: But-1,4-dc.

chosen for conversion of fugacity to pressure. The simulation box for all tasks consist of 32 unit cells. In other words, a construction of (2 × 4 × 4) cells was established for simulations to reach cutoff radius equal to a 12.5 Å criterion. In addition, periodic boundary conditions in three dimensions were used for all simulations. The long-range electrostatic interactions were also handled using the Ewald-summation technique.

3. Results and discussion

The reaction between butane-1,4-dicarboxylic acid and sodium azide with copper(II) nitrate led to formation of MFUM-1(Cu). Nano-sheets of MFUM-1(Cu) were obtained by ultrasonic irradiation, while single crystals of MFUM-1(Cu) were obtained under mild conditions. All synthetic procedures are shown in Scheme 1. Careful analysis shows that the crystal structure of MFUM-1(Cu) and the related nano-structures obtained by the sonochemical method are identical.

3.1. IR spectra

IR spectra of the nano-structures and single crystal of MFUM-1 (Cu) are indistinguishable and show a medium intense broad absorption in the 3167–3523 cm^{-1} range which is attributed to the lattice and coordinated H_2O. The bands at 1547, 1548 cm^{-1} and 1401–1404 cm^{-1} can be assigned to anti-symmetric $\nu_{as}(COO^-)$ and symmetric $\nu_s(COO^-)$ stretching vibrations. The resulting values of $\Delta\nu$ ($\Delta\nu = \nu_{as} - \nu_s$) are 146 and 144 cm^{-1} respectively. These $\Delta\nu$ values are characteristic of the bidentate bonding mode of the carboxylate group. Also, the sharp bands at 2088–2091 cm^{-1} are evidence of the existence of coordinated N_3^- anion.[30] These findings are supported by the solid-state structure obtained from X-ray diffraction measurements.

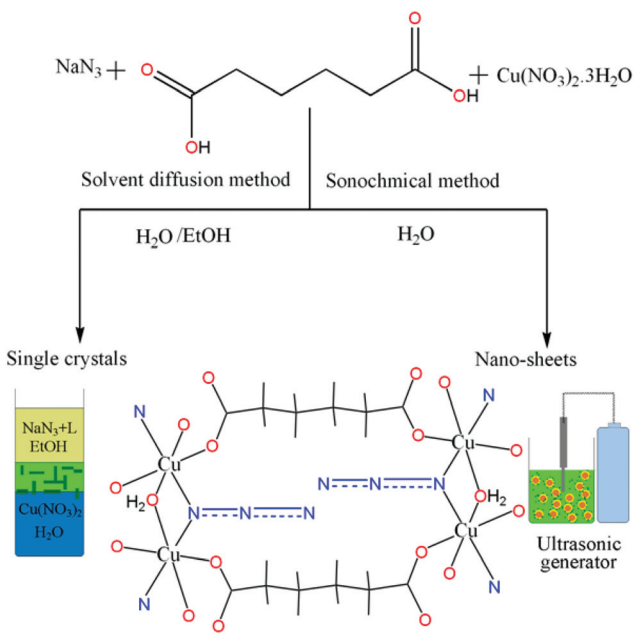

Scheme 1 The synthetic procedure of MFUM-1(Cu) and its nano-sheets.

3.2. Description of crystal structure

3.2.1. $\{[Cu(but\text{-}1,4\text{-}dc)_{0.5}(N_3)(H_2O)]\cdot H_2O\}_n$ (MFUM-1(Cu)). The X-ray crystal structure analysis reveals that MFUM-1(Cu) forms two-dimensional Cu-based MOF$\{[Cu(but\text{-}1,4\text{-}dc)_{0.5}(N_3)(H_2O)]\cdot H_2O\}_n$ that crystallizes in the monoclinic system with space group $C2/m$ (Table 1). As shown in Fig. 1, each Cu^{II} centre displays a distorted octahedral coordination geometry.

The octahedral sphere can be described as a basal plane associated with two N (Cu–N1, 2.015 (11) Å) and two O (Cu–O1, 1.959 (11) Å) atoms from two end-on (*EO*) azido and two $(but\text{-}1,4\text{-}dc)^{2-}$ bridging ligands respectively and axial positions occupied by two bridging water molecules (Cu–O2, 2.444 (1) Å). The propagation of the polymer is achieved through two centrosymmetric azido and H_2O bridges that bind to Cu centres forming one-dimensional double stranded chains of $[Cu_2(N_3)(H_2O)]_n$ along the *b*-axis (Fig. 2).

The azide bridges are quasi-linear with the N–N–N angle 178.63(2)° and adopt the *EO* coordination mode that, according to the current knowledge of magnetostructural correlations, should lead to ferromagnetic coupling along the 1D

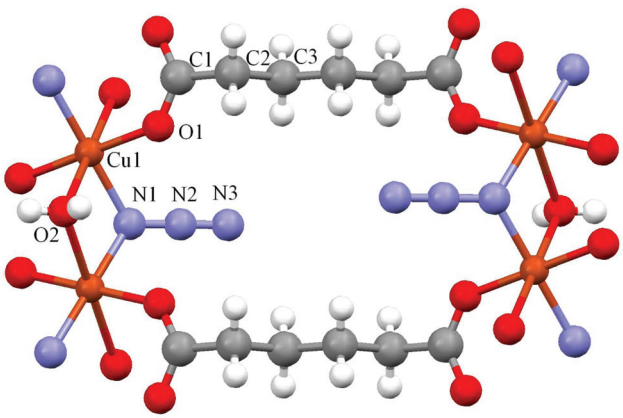

Fig. 1 Asymmetric unit of MFUM-1(Cu) with the atom numbering scheme.

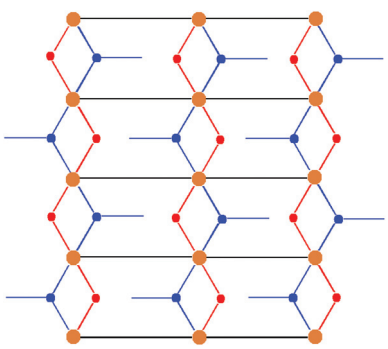

Fig. 2 Schematic view of one-dimensional double stranded chains of $[Cu_2(N_3)(H_2O)]_n$.

chain. Geometric parameters relevant to the magnetic properties are the θ bridge angle (θ = 106.89°), the Cu–N_{azide} bond length (2.015 (11) Å), and the Cu···Cu separation (3.24 Å). The $(But\text{-}1,4\text{-}dc)^{2-}$ co-ligand has a crucial dual role in constructing MFUM-1(Cu) (Table S1†). First, each carboxylate group acts as a three-atom bridge to link adjacent copper centres aligned with the azide and water molecules. Second, it acts as a bis-bidentate linker to connect 1D chains and extend the structure into a 2D layer network with square space in the *ab* plane (Fig. S1†). Parallel squares are connected by O–H···N hydrogen bonds into a ring having the graph-set notation $R_2^2(30)$ (O/N distance is 2.931(3) Å) to generate channels having a square aperture along the *c*-axis with a volume of 29.9 $Å^3$ or 4.2% of the unit cell (computed by Platon[31] (Fig. 3)). These channels are filled by the water molecules. It is worthwhile mentioning that although all pores are occupied with water molecules, they can be readily removed using heating in a vacuum oven in practical situations. That means, before doing any adsorption measurements, guest molecules such as water molecules are removed from pore structures and the pores could be accessible for adsorbate molecules. Therefore, here we also removed water molecules from structure pores in all performed simulations to real condition.

The guest water molecules located in the channels could not be exactly refined owing to severe disorder (refined occupancies of 0.513(12), 0.326(11) and 0.188(9) for O3, O4, and O5 respectively), as is common in microporous CPs and MOFs. Therefore, the identity and number of the guest molecules ($2H_2O$) in MFUM-1(Cu) was determined on the basis of thermogravimetric analysis (TGA) data. In addition, there are some O–H···O hydrogen bonds that make the solid-state structure of MFUM-1(Cu) more stable and assembled as a 3D network (Fig. 4).

CSD search. There are large numbers of coordination networks containing the azido bridge (1100 and 323 examples for *EO* and *EE* coordination modes respectively) in the Cambridge Structural Database (CSD version 5.38/Feb 2017) and most of them have magnetically active transition metals such as Cu, Ni, Mn, and Co as metal centres (Fig. S2†). Among them, dimer and polynuclear (*n* = 3–24) complexes have been extensively investigated, however studies on higher dimensional azido-bridged complexes are less usual (Fig. 5).

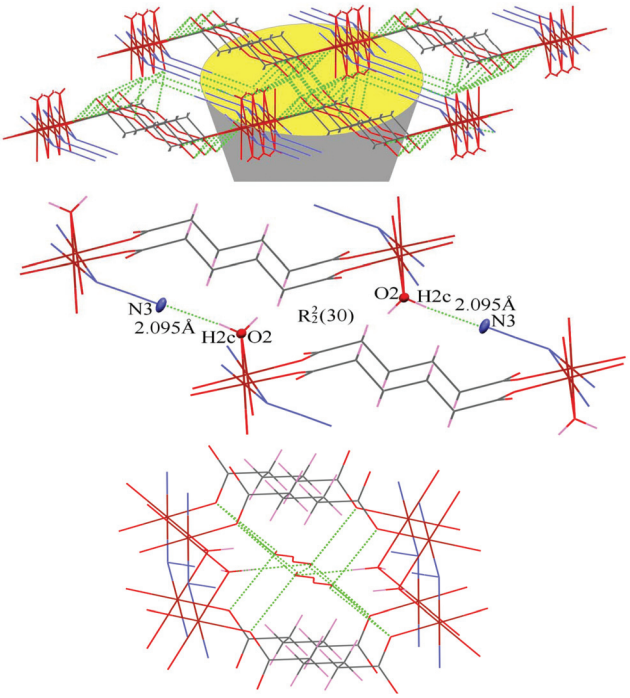

Fig. 4 Crystal packing of MFUM-1(Cu) showing the H-bonds along the *c*-axis with schematic representation of graph sets at the bottom of the figure.

Up to now, a common strategy for the design of high dimensional frameworks is to incorporate a second bridging ligand into the metal-azido complexes. For clarification, a statistical study was done on the second ligands in the azido-bridged complexes and the results showed that the most abundant are corresponded to neutral nitrogen donor and mono alcoholic or carboxylate ligands while those containing aliphatic based dicarboxylate ligands are the least in number (Fig. S3†). This is presumably due to the difficulty for negatively charged ligands to coexist in the same molecule with azide in the competition occurring in process of self-assembly. However, the synthesis and study of structures containing azide/dicarboxylate ligands are very interesting since dicarbox-

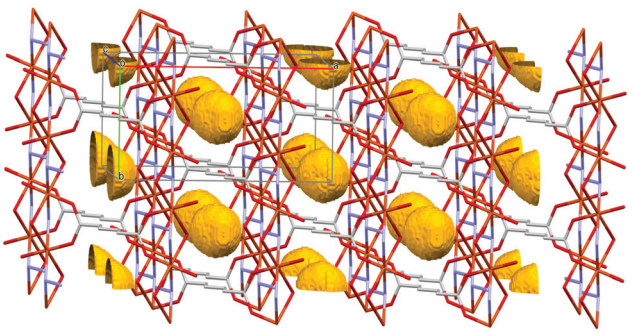

Fig. 3 Crystal packing of MFUM-1(Cu) showing square-shaped channels along the *c*-axis filled by water molecules.

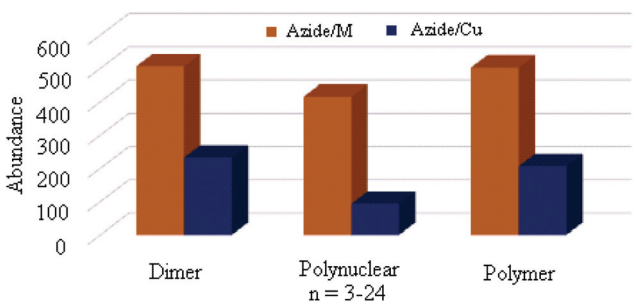

Fig. 5 Abundance of dimer, polynuclear (*n* = 3–24), and infinite polymeric complexes containing bridging azido ligand.

ylate ligands have the ability to connect metal-azido skeletons and form higher dimensional molecular nets. Table 3 presents all reported Cu coordination compounds with *EO*-azido bridge and dicarboxylate ligands. As can be seen, all structures are infinite 1D or 2D coordination networks. The Cu/azide systems with a Cu–N_{azide}–Cu angle (θ) ≤104° and a maximum Cu–N_{azide} bond length of 2.20 Å are ferromagnetically coupled. But the geometric parameters corresponding to the magnetic properties show behavior contrary to expectations as some of these compounds have antiferromagnetic behavior. These results clearly show that carboxylate bridges can modify the magnetic properties.

3.3. Role of experimental parameters on nano-structure of MFUM-1(Cu)

In order to achieve optimal conditions for the preparation of nano-structures of MFUM-1(Cu), seven experiments were designed (labeled A–G and summarized in Tables 2 and 4) and the effects of some parameters such as solvent, concentration and reaction time on the morphology and particle size were investigated.

3.3.1. Role of solvent. Solvent is one of the important factors that strongly influence the morphology and particle size of materials. Research shows that the dipole moment, vapor pressure, pH, and the ability to form hydrogen bonding of the selected solvent are cause of changes.[42] To investigate the effect of solvent on the sonochemical synthesis of MFUM-1 (Cu), we chose pure water, water–ethanol, and water–acetonitrile under A–C conditions. The PXRD patterns of the A and B products are shown in Fig. S4a–b.† The use of mixed water–acetonitrile solvent did not lead to the formation of product. As can be seen, the PXRD patterns of the A and B products match with the simulated PXRD derived from the single crystal study. SEM photographs are shown in Fig. S5a–b.† The crystal shape of A from pure water is nano-sheets with a thickness of 70–150 nm, whereas the crystals obtained from water–ethanol having a rod-shaped structure with a wide distribution of particle size (200 nm–2 μm). This change in morphology and size could be due to the polarity of the solvent and the effect of polarity can be understood by its ability to form hydrogen bonding interactions between the chemical groups emerging from the crystal surface and the solvent molecules. Generally, the solvent with greater hydrogen bonding interactions binds more strongly to the crystal surface leading to faster nucleation, delay in growth rate of the crystal faces, and reduction in particle size.[42] It is probable that interactions of the crystalline layers with solvent molecules are more favored compared to interactions directly between layers. In A, pure water is a polar protic solvent with a large dipole moment (1.87 Debye) and it is able to form many hydrogen bonds with small crystal surfaces. Thus, it prevents the agglomeration of particles and so limits the particle size. Adding ethanol to the water (with dipole moment 1.69 Debye) decreases number of hydrogen bonds due to the decrease in donor sites and there is a signifi-

Table 3 Comparison of geometric parameters corresponding to the magnetic properties for all Cu coordination compounds with EO-azido bridge and dicarboxylate ligands

Compounds	M–N_{azide} (Å)	M–O_{coo} (Å)	M···M(Å)	θ (°)	MB	D	Ref.
$\{[Cu_3(L)_2(N_3)_4]\cdot 7H_2O\}_n$	1.960, 1.980	1.953, 2.231	3.128	105.12	FO	2D	32
$[Cu(N_3)(tp)(CH_3OH)]_n$	2.006, 1.995	1.943, 1.953	3.185	105.53	FO	2D	33
$\{[Cu(but\text{-}1,4\text{-}dc)_{0.5}(N_3)(H_2O)]\cdot H_2O\}_n$	2.015	1.959	3.240	106.89	FO + AF	2D	MFUM-1(Cu)
$\{[Cu_2Dy(tda)_2N_3(H_2O)_4]\cdot 2H_2O\}_n$	2.116	1.972	3.345	104.44	FO	2D	34
$\{[Cu_3(bcpe)(N_3)_6]\cdot 2H_2O\}_n$	2.040, 2.600	1.947, 2.580	3.446	95.10	AF	2D	35
$\{[Cu(H_2O)_6][Cu_2(N_3)_{4/3}(OH)(pta)]\}_n$	2.286	1.984, 2.646	3.815	113.05	AF	2D	36
$\{Na_{10}[Cu_2(mpba)_2(N_3)_2]\cdot 18H_2O\}_n$	2.464	1.990,	4.353	123.92	AF + FO	2D	37
$[Cu_2(bcpb)(N_3)_4]_n\cdot nH_2O$	1.967, 1.986	1.956	3.098	103.18	FO + AF	1D	38
$[Cu_2(hmph)(N_3)_2(py)_2]_n$	1.978, 2.244	1.941, 1.996	3.327	103.81	AF	1D	39
$[Cu_2(N_3)_2(C_2O_4)(bpzm)_2]_n$	1.991, 2.524	1.991, 2.313	3.544	102.79	FO + AF	1D	40
$\{[Cu_3(DPA)_3(pzdc)(N_3)](ClO_4)_2\cdot 2H_2O\}_n$	2.336, 2.551	2.012, 2.515	3.793	101.72	AF	1D	41

MB = magnetic behavior, L = 1-carboxymethylpyridinium-4-benzoate, tp = terephthalate, tda = 2,3-dihydro-1*H*-1,2,3-triazole-4,5-dicarboxylato, bcpe = 1,2-bis(*N*-carboxymethyl-4-pyridinio)ethane, pta = phthalate, mpba = 1,3-phenylenebis(oxamato), bcpb = 1,4-bis(4-carboxylato-1-pyridinium)butane, hmph = homophthalate, bpzm = 1,1′-methylenebis(1*H*-pyrazole), py = pyridine, DPA = di(2-pyridylmethyl)amine, pzdc = pyrazole-3,5-dicarboxylate.

Table 4 Summary of results from different conditions of sonochemical synthesis

	A	B	C	D	E	F	G
Concentration (M) (Cu)	0.01	0.01	0.01	0.05	0.1	0.01	0.01
Solvent	H_2O	H_2O/EtOH	H_2O/CH_3CN	H_2O	H_2O	H_2O	H_2O
Reaction time (min)	40	40	40	40	40	20	60
Morphology	Nano-sheet	Rod shape	—	Plate	Rod shape	Rod shape	String-like
Average size	70–150 nm	200 nm–2 μm	—	200–500 nm	400 nm–2 μm	>2 μm	600 nm–2 μm
Yield (based on Cu)	71%	60.5%	—	74.5%	74.9%	55%	75.8%

cant growth in the crystal size. Also, the yields are more than obtained MFUM-1(Cu) by solvent diffusion method (see Table 4).

3.3.2. Role of initial reactant concentration. In order to investigate the effect of initial reactant concentration on the morphology and size of the sonochemical product, experiments were carried out at three different concentrations of copper salt (0.01, 0.05, and 0.1 M) under A, D and E conditions. The PXRD patterns of A, D and E products are shown in Fig. S6a, d and e.† A careful look at the diffraction patterns reveals an acceptable match between these and the simulated data (patterns). SEM photographs are shown in Fig. S7a, d and e.† The pictures clearly show that the nano-sheets of A (in a size range of 70–150 nm) agglomerate to form rod shape crystals of E (in a size range of 400 nm–2 μm) with increasing reactant concentration.

3.3.3. Role of reaction time. Ultrasonic syntheses of MFUM-1(Cu) for different reaction times of 20, 40, and 60 min were carried out under F, A, and G conditions. The PXRD patterns of the resulting products are shown in Fig. S8a, f, and g.† It is clearly seen that the peak positions in the experimental PXRD patterns of a and f are in good agreement with the corresponding simulated one (s), indicating the phase purity of A and F products. But for G, some diffraction peaks of an unknown phase appeared at 20 and 40.2 2θ when the reaction time was increased to 60 min, indicating that the crystal or molecular structure of the sample changed under ultrasound irradiation for a long time. The broadening and weakening of the diffraction peaks indicate that the samples are composed of small crystals with nanometer dimensions. The morphologies and size were characterized by SEM and the results are shown in Fig. S9a, f, g1 and g2.† Sample F was only sonicated for 20 min leading to the formation of rod shape crystals with a wide distribution of particle size which is often undesirable (Fig. S9f†). Fig. S9a† clearly shows that the increase of the reaction time to 40 min leads to uniformity and a decrease in the dimensions of the nano-sheets of MFUM-1(Cu) (the thickness range of 70–150 nm). When the reaction time is increased to 60 min, string-like crystals in a size range of 600 nm–2 μm are obtained. Furthermore, extending of reaction time to 60 min resulted in a significant increase in the yield of $\{[Cu(But\text{-}1,4\text{-}dc)_{0.5}(N_3)(H_2O)]\cdot H_2O\}_n$ to 75.8% compared with the solvent diffusion method. In summary, these results indicate that optimal conditions for the synthesis of nano-sheets of MFUM-1(Cu) is use of pure water as solvent, low concentration of reactants and reaction time of 40 min (A experiment, Table 4).

3.4. Thermogravimetric analyses (TGA)

To examine the thermal stability of the single crystals of the MFUM-1(Cu) and its nano-sheets, thermal gravimetric analyses (TGA) were performed from 5 to 1000 °C with a heating rate of 10 °C min^{-1} (see Fig. S10a and b†). The TG curve of MFUM-1 (Cu) in the range of 50–250 °C exhibits a two-step weight loss with an overall mass loss of 81.20% (Fig. S10a†). The weight loss of 16.00% (calcd: 16.97%) for the first stage occurs between 50 to 75 °C, which corresponds to two lattice water molecules. The second weight loss of 61.80% from 245–450 °C is ascribed to collapse of the network (calcd: 62.74%). These findings suggest that the host network may be stable up to 245 °C but then starts to suddenly lose its ligands as a result of thermal decomposition. The remaining weight (22.19%) corresponds to the percentage of Cu and O components, indicating that the final residue is CuO. Also, decomposition of nano-structure MFUM-1(Cu) starts about 17 degrees earlier (Fig. S10b†) than its single crystals, probably due to reduction of the particle size of the coordination polymer to a few dozen nanometers and a much higher surface to volume ratio that leads to lower thermal stability.

3.5. Gas separation and purification analysis

To investigate the potential application of MFUM-1(Cu) in gas separation processes, the GCMC simulation was employed for all isotherm predictions for three CO_2, CH_4 and N_2 industrial gases in a pressure range of 0–0.15 MPa and at a temperature of 298 K. Fig. 6 shows the calculated binary isotherms for CO_2/N_2 (15–85) and CO_2/CH_4 (50–50) real mixtures.

As it can be seen, the adsorption capacity for CO_2 is significantly higher than the other gases at all pressures implying MFUM-1(Cu) to be a promising candidate for CO_2 separation

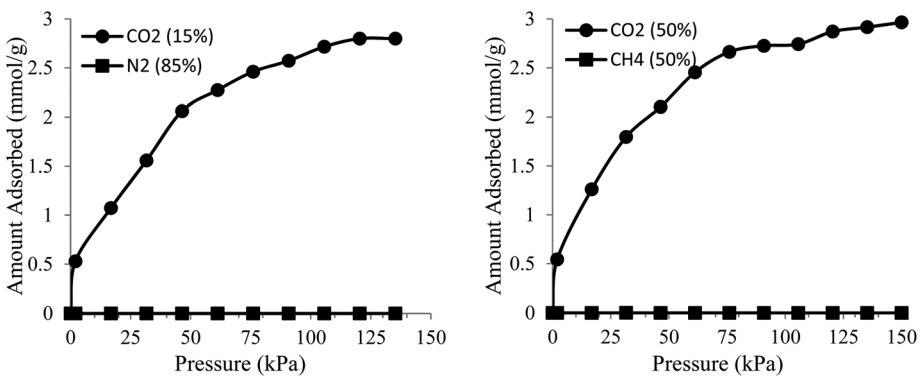

Fig. 6 Simulated adsorption isotherms of CO_2/N_2 (15–85) and CO_2/CH_4 (50–50) mixtures over MFUM-1(Cu) at 298 K.

over CH_4 and N_2. For a better understanding of the CO_2 capacity of MFUM-1(Cu), its adsorption capacity is compared with some of the best porous metal–organic framework adsorbents for CO_2 adsorption (Fig. S11†). It is obvious that the CO_2 capacity of MFUM-1(Cu) is acceptable as many MOFs provide the same adsorption capacity as our structure.

Worthwhile mentioning that the smaller particles favor higher and also fast uptake of gas mixtures owing to pore accessibility improvement.[43–45] However, it cannot be considered in our simulations because true and complete structure with full-empty pores is utilized. In addition to proper capacity, the effectiveness of an adsorbent for a certain separation process directly depends on the desired component selectivity. Therefore, the selectivity of CO_2 over the other components of the gas mixtures is calculated based on binary simulated isotherms (Fig. 6). As illustrated in Fig. 6, a significant difference in adsorption capacity for the gases is observed resulting in adsorptive selectivity (based on thermodynamic separation). The following equation should be used for evaluating the adsorptive selectivity.[20]

$$S = (q_1/q_2)/(P_1/P_2) \quad (1)$$

Based on eqn (1), the selectivity factor is defined as the molar ratio of the adsorption quantities at the relevant partial pressures of the gases. Table 5 compares the selectivity for CO_2 over N_2 and CH_4 for MFUM-1(Cu) in comparison with other porous materials such as MOFs. It should be noted that, the adsorption selectivity of CO_2 is calculated for an equimolar binary mixture of CO_2/CH_4 and a mixture of 15%:85% for CO_2/N_2. From Table 5, it can be observed that CO_2 selectivity in MFUM-1(Cu) is comparable to the best porous structures reported in the literature. Actually, the presence of the bridging azido ligand with high ionic potential in structure of MFUM-1(Cu) leads to the formation of strong partial charges which can interact with the quadrupole moment of CO_2. The electrostatic interactions between the quadrupole moments of CO_2 and active sites on the MFUM-1(Cu) makes it capable to be highly effective in trapping of CO_2 from a gas mixture of N_2 and CH_4. Obviously, MFUM-1(Cu) can be a promising candidate for industrial separation of CO_2/CH_4 andCO_2/N_2 real gas mixtures.

Table 5 Adsorptive selectivity of CO_2/N_2 and CO_2/CH_4 for MFUM-1 (Cu) in comparison with some porous MOFs and zeolites materials borrowed from literature[19,21,46]

Structure names	CO_2/CH_4 (50 : 50)	CO_2/N_2 (15 : 85)	T (K)
rho-MOF	500	19 000	298
MFUM-1(Cu)	192	7531	298
Soc-MOF	36	—	298
mmen-Cu-BTTri	—	165	298
HKUST-1	—	101	293
Mg-MOF-74	—	66.1	333
bio-MOF-11	—	65	298
en-Cu-BTTri	—	44	298
Mg-MOF-74	—	44	303
Cu-BTC	9	35	298
Ni-MOF-74	—	30	298
ZIF-78	—	30	298
Cu-TATB-60	—	24	298
ZIF-100	—	22	298
ZIF-69	7	22	298
Cu-BTTri	—	19	303
Fe-BTT	—	18	303
ZIF-68	6	17	298
MOF-508	6	6	298
IRMOF-1	3	—	298
MOF-177	—	4	298
MOF-253	—	9	298
MFI	20	30	298
DDR	20	38	298
FAU	10	20	298

3.6. Magnetic properties

Magnetic properties of MFUM-1(Cu) were measured for both the compound synthesized in the form of crystals and in the form of nano-sheets. The data for both these forms is consistent with each other. The product of molar magnetic susceptibility and temperature measured in 1 kOe plotted as a function of temperature for MFUM-1(Cu) in both forms is presented in Fig. 7. At room temperature, χT reaches a value of 0.61 cm^3 K mol^{-1}, which is slightly higher than the value predicted for one Cu atom with g = 2.2 and spin s = 1/2, equal to 0.45 cm^3 K mol^{-1}.χT exhibits a peak around 7 K to sharply drop at lower temperatures, indicating long-range ordering.

A Curie–Weiss law fit performed in the range 150–300 K (see Fig. 7, inset) yields a positive value of the Weiss temperature equal 35.4 K and 36.2 K for the crystalline form and nanosheets, respectively, and a value of the Curie constant 0.54 cm^3 K mol^{-1} in both cases, close to the previously calculated 0.45 cm^3 K mol^{-1}. The positive value of the Weiss temperature suggests ferromagnetic coupling between the Cu atoms through the bridging azido ligand. However, as can be seen in Fig. 8 in the magnetization *versus* field plot, M does not reach

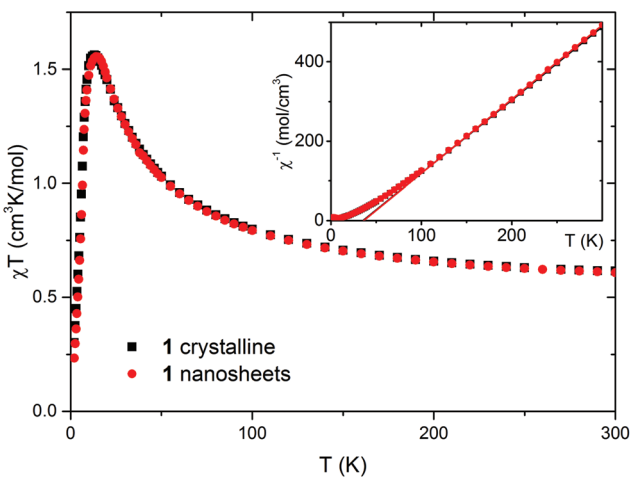

Fig. 7 The product of molar magnetic susceptibility and temperature of MFUM-1(Cu) in both crystalline and nano-sheets form as a function of temperature measured in 1 kOe. Inset: Inverse molar magnetic susceptibility of MFUM-1(Cu) in both forms measured in 1 kOe (the same colors and symbols used as in the $\chi T(T)$ plots) with Curie–Weiss fits performed in 150–300 K range (solid lines).

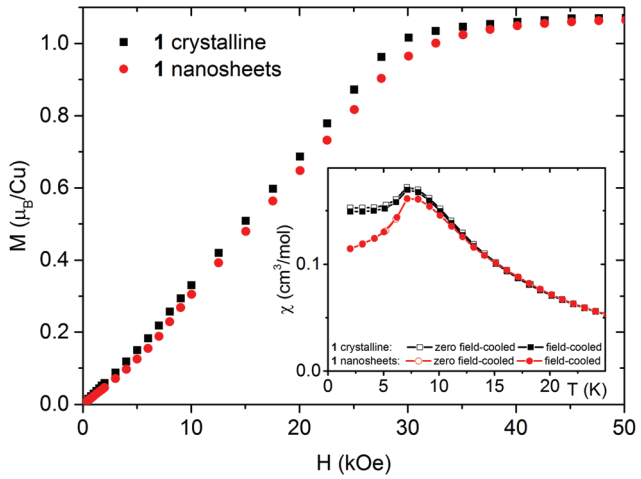

Fig. 8 Isothermal magnetization of MFUM-1(Cu) in crystalline and nano-sheets form per one Cu atom as a function of magnetic field measured at 1.8 K. Inset: Zero field-cooling/field cooling magnetic susceptibility of MFUM-1(Cu) in both forms, measured in 50 Oe. Solid lines are to guide the eye.

the saturation value in low magnetic fields – a clear spin–flip transition is seen in both cases around 23 kOe. The saturation value of 1.07μ_B/Cu for both forms agrees well with the theoretically predicted 1.1μ_B/Cu. Both the presence of the spin–flip transition and the characteristic peak in zero-field cooling/field cooling curves (see Fig. 8, inset), with no difference between respective zero field-cooled and field-cooled susceptibilities, indicate antiferromagnetic long-range ordering below 7.3 K. This is further confirmed by AC measurements for both forms (see ESI†): AC magnetic susceptibility *versus* temperature measured at four frequencies of the AC field shows no frequency dependence and no χ'', whereas at 7.3 K a clear peak is visible in χ' for both the crystalline form and nano-sheets. This, together with the positive Weiss temperature, indicates antiferromagnetic coupling between ferromagnetically coupled chains, antiferromagnetic coupling being weaker than the intrachain ferromagnetic interactions.

4. Conclusions

This work reports a novel magnetic mixed-ligand Cu-based MOF involving azido and (but-1,4-dc)$^{2-}$ bridging ligands, $\{[Cu(but\text{-}1,4\text{-}dc)_{0.5}(N_3)(H_2O)]\cdot H_2O\}_n$ (**MFUM-1(Cu)**). Structural analysis shows that one-dimensional water and EO azide-bridged Cu^{II} chains $[Cu_2(N_3)(H_2O)]_n$ are assembled through the bis-bidentate (but-1,4-dc)$^{2-}$ linker to form a 2D layer architecture in MFUM-1(Cu). Apparently, the structure consists of a 3D polymeric network with long channels with a 29.9 Å^3 or 4.2% of the unit cell volume. In these channels, disordered water molecules are present (these waters refine properly with free occupancy factors). The porous structure makes MFUM-1 (Cu) an excellent candidate for applications in gas separations. GCMC simulation shows that the adsorption capacity and selectivity of CO_2 for the MFUM-1(Cu) is comparable with the best reported porous structures in the literature. Additionally, to determine the changes in physical properties depending on the size (such as thermal stability), nano-sheets of MFUM-1 (Cu) were prepared by sonochemical method and role of some experimental parameters such as solvent, concentration and reaction time on the morphology and size of product was studied. Magnetic measurements showed intrachain ferromagnetic and interchain antiferromagnetic coupling between the Cu atoms. Overall, such a study expands the chemistry of the azide/aliphatic based dicarboxylate systems that are rare and can help to better understanding of magnetostructural correlations in these structures.

Conflicts of interest

There are no conflicts to declare.

Acknowledgements

M. M. wishes to thank to the Ferdowsi University of Mashhad for financial support of this article (Grant No. 28392/3). A. M. acknowledges financial support from the Polish National Science Centre within the SONATA Project UMO-2015/19/D/ST5/01936. M. M. gratefully acknowledges the Cambridge Crystallographic Data Centre (CCDC) for access to the Cambridge Structural Database.

References

1 (*a*) O. Kahn, *Molecular Magnetism*, Wiley-VCH, Weinheim, 1993; (*b*) R. L. Carlin, *Magnetochemistry*, Springer, Heidelberg, 1986, ch. 7; (*c*) H.-L. Sun, Z.-M. Wang and S. Gao, $[M(N_3)_2(H_2O)_2]\cdot$(bpeado): Unusual Antiferromagnetic Heisenberg Chain (M=Mn) and Ferromagnetic Ising Chain (M=Co) with Large Coercivity and Magnetic Relaxation (bpeado = 1,2-Bis(4-pyridyl) ethane-N,N′-dioxide), *Chem. – Eur. J.*, 2009, **15**, 1757–1764.

2 X.-Y. Wang, Z.-M. Wang and S. Gao, Constructing magnetic molecular solids by employing three-atom ligands as bridges, *Chem. Commun.*, 2008, 281–294.

3 J. S. Miller and M. Drillon, *Magnetism: Molecules to Materials IV*, Wiley-VCH, Verlag GmbH, 2002.

4 (*a*) X.-J. Li, X.-Y. Wang, S. Gao and R. Cao, Two Three-Dimensional Metal–Organic Frameworks Containing One-Dimensional Hydroxyl/Carboxylate Mixed Bridged Metal Chains: Syntheses, Crystal Structures, and Magnetic Properties, *Inorg. Chem.*, 2006, **45**, 1508–1516; (*b*) M.-H. Zeng, Y.-L. Zhou, M.-C. Wu, H.-L. Sun and M. Du, A unique cobalt(II)-based molecular magnet constructed of hydroxyl/carboxylate bridges with a 3D pillared-layer motif, *Inorg. Chem.*, 2010, **49**, 6436–6442.

5 (*a*) S. Tanase and J. Reedijk, Chemistry and magnetism of cyanido-bridged d–f assemblies, *Coord. Chem. Rev.*, 2006, **250**, 2501–2510; (*b*) M. Atanasov, P. Comba, G. R. Hanson, S. Hausberg, S. Helmle and H. Wadepohl, Cyano-bridged homodinuclear copper(II) complexes, *Inorg. Chem.*, 2011, **50**, 6890–6901; (*c*) M. B. Zakaria, M. S. A. Hossain, M. J. A. Shiddiky, M. Shahabuddin, E. Yanmaz, J. H. Kim, A. A. Belik, Y. Ide, M. Hu, S. Tominaka and Y. Yamauchi, Cyano-Bridged Trimetallic Coordination Polymer Nanoparticles and Their Thermal Decomposition into Nanoporous Spinel Ferromagnetic Oxides, *Chem. – Eur. J.*, 2016, **22**, 15042–15048.

6 (*a*) J. Ribas, A. Escuer, M. Monfort, R. Vicente, R. Cortés, L. Lezama and T. Rojo, Polynuclear NiII and MnII azido bridging complexes. Structural trends and magnetic behavior, *Coord. Chem. Rev.*, 1999, **193–195**, 1027–1068; (*b*) C. Adhikary and S. Koner, Structural and magnetic studies on copper(II) azido complexes, *Coord. Chem. Rev.*, 2010, **254**, 2933–2958; (*c*) Y.-Q. Wang, Q.-H. Tan, X.-Y. Guo, H.-T. Liu, Z.-L. Liu and E.-Q. Gao, Novel manganese(II) and cobalt(II) 2D polymers containing alternating chains with mixed azide and carboxylate bridges: crystal structure and magnetic properties, *RSC Adv.*, 2016, **6**, 72326–72332; (*d*) X. Liu, P. Cen, F. Li, X. Ma, H. Zhou, X. Chen, W. Song, G. Xie and S. Chen, A unusual two-dimensional azido-Cu(II) network with benzoate derivative as a co-ligand exhibiting ferromagnetic order and slow magnetic relaxation, *RSC Adv.*, 2016, **6**, 96103–96108; (*e*) A. Escuer, R. Vicente, M. S. E. Fallah, M. Font-Bardia and A. Escuer, A Ferromagnetic Salicylaldoximate/Azide $Mn^{II}{}_2Mn^{III}{}_6$ Cluster with an S=17 Ground State and a Single-Molecule-Magnet Response, *Inorg. Chem.*, 2016, **55**, 5735–5737.

7 (*a*) E. Pardo, C. Train, R. Lescouëzec, K. Boubekeur, E. Ruiz, F. Lloret and M. Verdaguer, Synthesis, crystal structure and magnetic properties of two oxalato-bridged dimetallic trinuclear complexes combined with a polar cation, *Dalton Trans.*, 2010, **39**, 4951–4958; (*b*) G. Marinescu, D. Visinescu, A. Cucos, M. Andruh, Y. Journaux, V. Kravtsov, Y. A. Simonov and J. Lipkowski, Oxalato-Bridged $[Cu^{II}Cr^{III}]$ and $[Mn^{II}Cr^{III}]$ Binuclear Complexes: Synthesis, Crystal Structures, Magnetic and EPR Investigations, *Eur. J. Inorg. Chem.*, 2004, 2914–2922.

8 (*a*) X. Chen, A. L. Cui and C. M. Liu, Synthesis, structures, and magnetic properties of carboxylate-bridged trinuclear complexes based on low-spin manganese(III)/iron(III) building blocks, *Transition Met. Chem.*, 2013, **38**, 683–688; (*b*) G.-M. Zhuang, X.-B. Li, Y.-Q. Wen, C.-Y. Tian and E.-Q. Gao, Structures and Magnetic Properties of Manganese(II) Compounds Based on Chains with Simultaneous Carboxylate and Pseudohalide Bridges, *Eur. J. Inorg. Chem.*, 2014, 3488–3498.

9 Y. Song, C. Massera, M. Quesada, A. M. ManottiLanfredi, I. Mutikainen, U. Turpeinen and J. Reedijk, A one-dimensional copper (II) coordination polymer $[Cu_3(ampym)_2(\mu1,1\text{-}N_3)_4(\mu1,3\text{-}N_3)_2(dmf)_2]n$ (ampym = 2-aminopyrimidine) containing both end-on and end-to-end azido bridges, *Inorg. Chim. Acta*, 2005, **358**, 1171–1178.

10 Q. Yang, X.-F. Zhang, J.-P. Zhao, B.-W. Hu and X.-H. Bu, Cobalt (II)–Azido Coordination Polymers with Dicarboxylate and Di(1H-imidazol-1-yl)methane Ligands Exhibiting Ferromagnetic Behaviors, *Cryst. Growth Des.*, 2011, **11**, 2839–2845.

11 G. Mínguez Espallargas and E. Coronado, Magnetic functionalities in MOFs: from the framework to the pore, *Chem. Soc. Rev.*, 2018, **47**, 533–557.

12 M. Kurmoo, Magnetic metal–organic frameworks, *Chem. Soc. Rev.*, 2009, **38**, 1353–1379.

13 M. Peller, K. Böll, A. Zimpel and S. Wuttke, Metal–organic framework nanoparticles for magnetic resonance imaging, *Inorg. Chem. Front.*, 2018, **5**, 1760–1779.

14 J. K. Nath, A. Mondal, A. K. Powell and J. B. Baruah, Structures, Magnetic Properties, and Photoluminescence of Dicarboxylate Coordination Polymers of Mn, Co, Ni, Cu Having N-(4-Pyridylmethyl)-1,8-naphthalimide, *Cryst. Growth Des.*, 2014, **14**(9), 4735–4748.

15 (*a*) C. G. Carson, A. J. Brown, D. S. Sholl and S. Nair, Sonochemical Synthesis and Characterization of Submicrometer Crystals of the Metal–Organic Framework $Cu[(hfipbb)(H_2hfipbb)_{0.5}]$, *Cryst. Growth Des.*, 2011, **11**, 4505–4510; (*b*) A. Morsali, H. Hosseini Monfared, A. Morsali and C. Janiak, Ultrasonic irradiation assisted syntheses of one-dimensional di (azido)-dipyridylamine Cu(II) coordination polymer nanoparticles, *Ultrason. Sonochem.*, 2015, **23**, 208–211; (*c*) H. Sadeghzadeh and A. Morsali, Hedge balls nano-structure of a mixed-ligand lead(II) coordination polymer; thermal, structural and X-ray powder diffraction studies, *CrystEngComm*, 2010, **12**, 370–372.

16 N. H. Ince, G. Tezcanli, R. K. Belen and I. G. Apikyan, Ultrasound as a catalyzer of aqueous reaction systems: the state of the art and environmental applications, *Appl. Catal., B*, 2001, **29**, 167–176.

17 R. V. Kumar, R. Elgamiel, Y. Diamant and A. Gedanken, Sonochemical preparation and characterization of nanocrystalline copper oxide embedded in poly (vinyl alcohol) and its effect on crystal growth of copper oxide, *Langmuir*, 2001, **17**, 1406–1410.

18 (*a*) J. Duan, Q. Li and L. Zhiyong, A new mesoporous coordination polymer: synthesis, structure, and gas adsorption studies, *CrystEngComm*, 2015, **17**, 2087–2090; (*b*) D. M. D'Alessandro, B. Smit and R. J. Long, Carbon dioxide capture: prospects for new materials, *Angew. Chem., Int. Ed.*, 2010, **49**, 6058–6082; (*c*) B. Li, H.-M. Wen, W. Zhou and B. Chen, Porous metal–organic frameworks for gas storage and separation: what, how, and why?, *J. Phys. Chem. Lett.*, 2014, **5**, 3468–3479.

19 B. Liu and B. Smit, Molecular Simulation Studies of Separation of CO_2/N_2, CO_2/CH_4, and CH_4/N_2 by ZIFs, *J. Phys. Chem. C*, 2010, **114**, 8515–8522.

20 J.-R. Li, J. R. Kuppler and H.-C. Zhou, Selective gas adsorption and separation in metal–organic frameworks, *Chem. Soc. Rev.*, 2009, **38**, 1477–1504.

21 K. Sumida, D. L. Rogow,, A. J. Mason, T. M. McDonald, D. E. Bloch, Z. R. Herm,, T.-H. Bae and J. R. Long, Carbon dioxide capture in metal–organic frameworks, *Chem. Rev.*, 2012, **112**, 724–781.

22 (*a*) A. Najafi, M. Mirzaei, A. Bauzá, J. T. Mague and A. Frontera, The roles of H-bonding, π-stacking, and antiparallel CO···CO interactions in the formation of a new Gd (III) coordination polymer based on pyridine-2,6-dicarboxylic acid, *Inorg. Chem. Commun.*, 2017, **83**, 24–26; (*b*) M. Shahbazi, F. Mehrzad, M. Mirzaei, H. Eshtiagh Hosseini, J. T. Mague, M. Ardalani and M. Shamsipur, Synthesis, single crystal X-ray characterization, and solution studies of Zn(II)-, Cu(II)-, Ag(I)- and Ni(II)-pyridine-2,6-dipicolinate N-oxide complexes with different topologies and coordination modes, *Inorg. Chim. Acta*, 2017, **458**, 84–96; (*c*) M. Alipour, O. Akintola, A. Buchholz, M. Mirzaei, H. Eshtiagh Hosseini, H. Görls and W. Plass, Size Dependent Self Assembly of Lanthanide Based Coordination Frameworks with Phenanthroline 2,9-dicarboxylic Acid as a Preorganized Ligand in Hybrid Materials, *Eur. J. Inorg. Chem.*, 2016, 5356–5365; (*d*) M. Mirzaei, H. Eshtiagh Hosseini, M. Alipour, A. Bauzá, J. T. Mague, M. Korabik and A. Frontera, Hydrothermal synthesis, X-ray structure and DFT and magnetic studies of a (H 2 SiW 12 O 40) 2− based one-dimensional linear coordination polymer, *Dalton Trans.*, 2015, **44**, 8824–8832; (*e*) M. Mirzaei, H. Eshtiagh Hosseini, Z. Karrabi, B. Notash, A. Bauzá and A. Frontera, Synthesis, structure and DFT study of a chelidamic acid based Cu coordination polymer: On the importance of π–π interactions and hexameric water clusters, *J. Mol. Struct.*, 2015, **1080**, 30–36; (*f*) M. Mirzaei, H. Eshtiagh Hosseini, Z. Karrabi and B. Notash, catena-Poly[[di-[μ]$_2$-aqua-hexaaquabis-([μ]$_3$-4-oxido-pyridine-2,6-dicarboxyl-ato)tri-manganese(II)] trihydrate]: a new one-dimensional coordination polymer based on a trinuclear MnII complex of chelidamic acid, *Acta Crystallogr., Sect. C: Cryst. Struct. Commun.*, 2013, **69**, 1140–1143; (*g*) M. Mirzaei, H. Eshtiagh-Hosseini, A. Hassanpoor, T. Szymańska-Buzar, J. T. Mague, M. Korabik and A. Kochel, Two new Cu^{II} 1D-coordination polymers containing 1,4-pyrazine-2,3-dicarboxylic acid, 2-aminopyridine, and 5-bromo-6-methyl-2-(4-methylpiperazine-1-yl)pyrimidine-4-amine: X-ray crystal structure, spectroscopic and magnetic studies, *Inorg. Chim. Acta*, 2012, **391**, 232–238; (*h*) M. Mirzaei, H. Eshtiagh-Hosseini, A. Hassanpoor and V. Barba, X-ray structure of 1D-coordination polymer of copperII bearing 1, 4-pyrazine-2, 3-dicarboxylic acid and 2-aminopyrimidine, *J. Serb. Chem. Soc.*, 2012, **77**, 67–73; (*i*) A. Hassanpoor, M. Mirzaei, H. Eshtiagh-Hosseini and A. Majcher, Constructing two 1D–coordination polymers and one mononuclear complex by pyrazine- and pyridinedicarboxylic acids under mild and sonochemical conditions: Magnetic and CSD studies, *CrystEngComm*, 2018, **20**, 3711–3721; (*j*) A. Hassanpoor, M. Mirzaei and H. Eshtiagh-Hosseini, Syntheses and characterization of two new coordination compounds containing an azide ligand in the presence of o-donor co-ligands with nickel and copper(II) metal ions and an investigation into the effects of sonochemical methods on morphology and particle size, *J. Iran. Chem. Soc.*, 2018, **15**, 1287–1292.

23 S. Koda, T. Kimura, T. Kondo and H. Mitome, A standard method to calibrate sonochemical efficiency of an individual reaction system, *Ultrason. Sonochem.*, 2003, **10**, 149–156.

24 O. V. Dolomanov, L. J. Bourhis, R. J. Gildea, J. A. K. Howard and H. Puschmann, OLEX2: a complete structure solution, refinement and analysis program, *J. Appl. Crystallogr.*, 2009, **42**, 339–341.

25 G. M. Sheldrick, Crystal structure refinement with SHELXL, *Acta Crystallogr., Sect. A: Found. Crystallogr.*, 2008, **64**, 112–122.

26 G. A. Bain and J. F. Berry, Diamagnetic corrections and Pascal's constants, *J. Chem. Educ.*, 2008, **85**, 532–536.

27 D. Frenkel and B. Smit, *Understanding Molecular Simulation: From Algorithms to Applications*, Elsevier, 2th edn, 2002, ISBN: 978-0-12-267351-1.

28 A. K. Rappe, C. J. Casewit, K. S. Colwell, W. A. Goddard and W. M. Skiff, UFF, a full periodic table force field for molecular mechanics and molecular dynamics simulations, *J. Am. Chem. Soc.*, 1992, **114**, 10024–10035.

29 T. Ogawa and T. Nakano, The Extended Universal Force Field (XUFF): Theory and Applications, *Chem-Bio Inf. J.*, 2010, **10**, 111–133.

30 K. Nakamoto, *Infrared Raman Spectra of Inorganic Coordination Compounds, Part B*, Wiley, New York, 5th edn, 1997.

31 PLATON: A. L. Spek, *Acta Crystallogr., Sect. D: Biol. Crystallogr.*, 2009, **65**, 148–155.

32 X.-M. Zhang, D.-D. Ding, W. Gao and J.-P. Liu, Structures and magnetism of metal(II) compounds with mixed azide and carboxylate bridges derived from zwitterionic dicarboxylate ligands, *Inorg. Chim. Acta*, 2013, **394**, 494–500.

33 Y.-F. Han, T.-W. Wang, Y. Song, Z. Shen and X.-Z. You, A 2D CuII complex containing ferromagnetically coupled 1D chain with threefold bridging ligands, *Inorg. Chem. Commun.*, 2008, **11**, 207–210.

34 X. Jiang, S.-D. Han, R. Zhao, J. Xu and X.-H. Bu, Ln III ion dependent magnetism in heterometallic Cu–Ln complexes based on an azido group and 1, 2, 3-triazole-4, 5-dicarboxylate as co-ligands, *RSC Adv.*, 2015, **5**, 62319–62324.

35 Y. Ma, Y.-Q. Wen, J.-Y. Zhang, E.-Q. Gao and C.-M. Liu, Structures and magnetism of azide-and carboxylate-bridged metal (II) systems derived from 1, 2-bis (N-carboxymethyl-4-pyridinio) ethane, *Dalton Trans.*, 2010, **39**, 1846–1854.

36 Y.-F. Zeng, X. Hu, J.-P. Zhao, B.-W. Hu, E. C. Sanudo, F.-C. Li and X.-H. Bu, Partial substitution of hydroxyl by azide: an unprecedented 2D azido–copper–hydroxyl compound with a [Cu$_{24}$] macrocycle in the presence of $[Cu(H_2O)_6]^{2+}$, *Chem. – Eur. J.*, 2008, **14**, 7127–7130.

37 X. Qu, X. Song, W. Li, Y. Xu, L. Li, D. Liao and Z. Jiang, Structural and magnetic properties of two copper(II) com-

plexes based on dinuclear copper(II) metallacyclophane, *Eur. J. Inorg. Chem.*, 2008, 1287–1292.

38 K. Wang, X.-C. Yi, X. Wang, X.-B. Li and E.-Q. Gao, Structures and magnetic properties of copper(II) and manganese(II) polymers derived from *pseudo*halides and a flexible zwitterionic dicarboxylate ligand, *Dalton Trans.*, 2013, **42**, 8748–8760.

39 J. Ma, D.-F. Wang, L.-Q. Fan and K. Zhou, Structure and magnetic properties of a copper (II) coordination polymer based on azide, pyridine and homophthalic acid, *Acta Crystallogr., Sect. C: Struct. Chem.*, 2015, **71**, 969–974.

40 A. Świtlicka-Olszewska, B. Machura and J. Mroziński, Synthesis, magnetic behavior and structural characterization of novel one-dimensional copper(II) coordination polymer based on azide and oxalate bridges, *Inorg. Chem. Commun.*, 2014, **43**, 86–89.

41 S. S. Massoud, F. R. Louka, L. T. Nguyen, M. Mikuriya, J. H. Albering and F. A. Mautner, Structural and magnetic characterization of 1-D complexes constructed from pyrazole-3, 5-dicarboxylate bridging multi copper(II) centers, *Inorg. Chim. Acta*, 2011, **366**, 394–398.

42 (*a*) I. Hod, Y. Mastai and D. D. Medina, Effect of solvents on the growth morphology of DL-alanine crystals, *CrystEngComm*, 2011, **13**, 502–509; (*b*) C. Sudha and K. Srinivasan, Understanding the effect of solvent polarity on the habit modification of monoclinic paracetamol in terms of molecular recognition at the solvent crystal/interface, *Cryst. Res. Technol.*, 2014, **49**, 865–872; (*c*) F. Shen, P. Lv, C. Sun, R. Zhang and S. Pang, The Crystal Structure and Morphology of 2,4,6,8,10,12-Hexanitro-2,4,6,8,10,12-hexaazaisowurtzitane (CL-20) p-Xylene Solvate: A Joint Experimental and Simulation Study, *Molecules*, 2014, **19**, 18574–18589; (*d*) L. Zhang, L.-H. Yue, F. Wang and Q. Wang, Divisive Effect of Alcohol– Water Mixed Solvents on Growth Morphology of Calcium Carbonate Crystals, *J. Phys. Chem. B*, 2008, **112**, 10668–10674; (*e*) V. Natarajan, M. Arivanandhan, K. Sankaranarayanan and Y. Hayakawa, Effect of pure and mixed solvents on the solubility, crystal growth and morphology of ethyl *p*-dimethylamino benzoate (EDMAB): An organic nonlinear optical material, *Physica B*, 2011, **406**, 1410–1414.

43 X. Fan, J. Zhou, T. Wang, J. Zheng and X. Li, Opposite particle size effects on the adsorption kinetics of ZIF-8 for gaseous and solution adsorbates, *RSC Adv.*, 2015, **5**, 58595–58599.

44 H. Han, Y. Cao, S. Chen, J. Lu, C. Huang, H. Zhu, P. Zhan and Y. Gao, Influence of particle size on gas-adsorption experiments of shales: An example from a Longmaxi Shale sample from the Sichuan Basin, China, *Fuel*, 2016, **186**, 750–757.

45 Y. Chen, L. Wei, M. Mastalerz and A. Schimmelmann, The effect of analytical particle size on gas adsorption porosimetry of shale, *Int. J. Coal Geol.*, 2015, **138**, 103–112.

46 R. Babarao and J. Jiang, Unprecedentedly High Selective Adsorption of Gas Mixtures in rho Zeolite-like Metal–Organic Framework: A Molecular Simulation Study, *J. Am. Chem. Soc.*, 2009, **131**, 11417–11425.

